



 Cite this: *RSC Adv.*, 2022, 12, 14477

Micellization and thermodynamics study of ester functionalized picoline-based ionic liquid surfactants in water†

 Dong Fu,^{‡,ab} Xiaoru Gao,^{‡,c} Jue Wang,^a Haijian Jiang,^a Mingming Zheng,^a Peng Li,^a Bo Huang,^a Kan Kan ^{*a} and Xiaochen Zhang^{*a}

A novel series of picoline-based ionic liquid surfactants, *N*-alkyloxycarbonyl-3-picoline bromides [C_{*n*}Empy][Br] (*n* = 10, 12, 14), have been synthesized. The thermal stability, aggregation behavior and surface activity of the synthetic ionic liquid surfactants were investigated systematically through a series of methods, such as thermogravimetric analysis (TGA), differential scanning calorimetry (DSC), tensiometry and conductivity. The thermodynamics of micellization of the ionic liquid surfactants solution were studied by using the conductivity method in the temperature range 278.15–318.15 K. The surface activity parameters and thermodynamics parameters were derived, respectively. The enthalpy–entropy compensation effect was further discussed by using relative thermodynamics parameters. It was found that the [C_{*n*}Empy][Br] have moderate surface activity, and their critical micelle concentration (CMC) decreased with the ester-functionalized chain length and exhibited a U-shape with temperature. The calculation results of the thermodynamic parameters showed that the micellization processes of [C_{*n*}Empy][Br] were spontaneous, endothermic at low temperature and exothermic at higher temperature.

Received 16th March 2022

Accepted 29th April 2022

DOI: 10.1039/d2ra01706g

rsc.li/rsc-advances

1. Introduction

Ionic liquids are a class of salts composed of organic cations and organic or inorganic anions with low melting points (<100 °C) that have been widely investigated for their unique physicochemical properties in recent years.^{1–3} Ionic liquids containing long alkyl groups are similar to cationic quaternary ammonium-based surfactants, which can self-assemble in water due to the intrinsic molecular nature.⁴ Many literature studies have reported a number of applications of amphiphilic ionic liquid self-assembly, such as liquid–solid extraction,⁵ synthesis of multi-walled carbon nanotubes,⁶ phase-transfer catalysis,⁷ gene delivery,⁸ and dispersal of petroleum asphaltenes.⁹ Thus, the analysis and investigation of the aggregation behavior of ionic liquid surfactants (ILs) is crucial to expand their application possibilities in various fields.

Aggregation behavior of ILs and the mixed micellization behavior of ILs with conventional surfactants in aqueous solution had been intensively investigated.^{10–18} Most of the

researches used long alkyl-chains ILs, which were not biodegradable and environmentally unacceptable compounds. Moreover, there are only a few investigations on the micellization behavior of the picoline-based ILs.^{10,19–24} Nowadays, the sustainable development of environment has become the primary concern of the research and development of novel surfactants. Researchers around the world are trying to develop the surfactants that are environmentally friendly and easily biodegradable. A number of papers reported that the ester functionalized of the hydrophobic chain could significantly improve the biodegradability of ILs compared with those containing simple alkyl chains.^{25,26} However, these researches mainly focused on the basic micellization behavior and anti-bacterial activity. The effect of ester functionalized chain length on the thermodynamics of micellar process had not been systematically investigated over a wide temperatures range. Therefore, the synthesis and systematic research on micellar process of the new ester-functional ILs could be a significant contribution to the development and understanding of the surfactants.

Reviewing our past work and understanding on alkylpicoline-based ILs,^{27,28} we have attempted to synthesize ester-functionalized picoline-based ILs by using natural molecules fatty acids and halogenated alcohol. As part of the research on aggregation behavior and surface activity of ester-functionalized ILs in water, this work aims to investigate the effect of ester-functionalized chain length on the thermodynamics of micellar process in a wide temperature range. A new

^aHeilongjiang Academy of Sciences, Institute of Advanced Technology, Harbin, P. R. China. E-mail: kankan.has@foxmail.com; 13946165731@163.com

^bCollege of Materials Science and Chemical Engineering, Harbin Engineering University, Harbin, P. R. China

^cHarbin Fiber Reinforced Plastic Institute, Harbin, P. R. China

† Electronic supplementary information (ESI) available. See <https://doi.org/10.1039/d2ra01706g>

‡ Dong Fu and Xiaoru Gao contributed equally to this work.



series of ester-functionalized picoline-based ILs were studied: *N*-alkoxy carbonyl-3-picoline bromides $[C_n\text{Empy}][\text{Br}]$ ($n = 10, 12, 14$). The aggregation behavior of ILs solutions were investigated by several methods, the surfactivity parameters of ILs were obtained. The conductivity test was conducted to investigate at a wide temperature range, and that the thermodynamic parameters of micellization process were characterized. This study provides theoretical basis for the application and development of ester functionalized picoline-based ionic liquids surfactants.

2. Experimental section

2.1 Reagents

Decanoic acid (98%), dodecanoic acid (97%), myristic acid (98%), 2-bromoethanol (98%), sulfuric acid (98%), 3-picoline (98%), toluene (98%), methyl trichloride (98%), anhydrous sodium sulfate (98%), methanol (98%) and ethyl acetate (98%) were purchased from Aladdin Reagent, all reagents were analytical grade. Deionized water was prepared by using Milli-Q (Millipore, USA).

2.2 Structural characterization of $[C_n\text{Empy}][\text{Br}]$

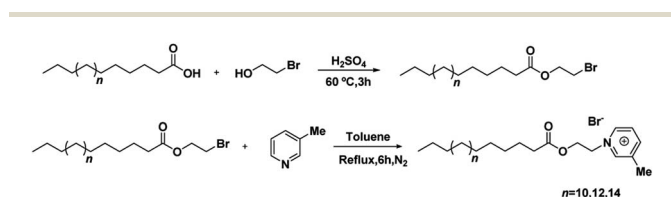
FT-IR was measured by attenuated total reflectance infrared spectroscopy on an Agilent Cary 630 spectrometer (Agilent, America) in the spectral range of 4000–660 cm^{-1} for each sample. ^1H NMR and ^{13}C NMR spectra were recorded on a Bruker Avance 600 MHz (Bruker, Germany), each sample was dissolved in CDCl_3 containing internal standard tetramethylsilane (TMS).

2.3 Thermal stability measurements

The thermal stability properties of the ILs were evaluated on a TG 209 F3 and a DSC 204 F1 (Netzsch, Germany), scanning to 500 °C at nitrogen atmosphere with a heating rate of 10 °C min^{-1} . All samples were measured at 3 times to confirm the uncertainty of the measurement.

2.4 Synthesis of ILs

The ILs were synthesized by two-step. First, the commercially available long-chain fatty acids were reacted with 2-bromoethanol to form the desired alkylating agents. Subsequently, the alkylating agents reacted with 3-picoline to form the picoline-based ILs. The synthetic process and spectra of the ILs were given in the ESI.† The general synthetic pathways were shown as follows (Scheme 1):



Scheme 1 The general synthetic pathways of $[C_n\text{Empy}][\text{Br}]$.

2.5 Surfactivity measurement of $[C_n\text{Empy}][\text{Br}]$

The surface tension of $[C_n\text{Empy}][\text{Br}]$ were made at 298.15 ± 0.10 K by the Du Noüy method using a tensiometer (Changji SYD-6541A, China). Glass containers were soaked in chromic acid solution and then washed at least 5 times with deionized water in order to remove any residual deposits. The platinum ring was heating over an alcoholic flame before each measurement. All samples were measured at least 5 times until the measuring results deviation was within ± 0.01 mN m^{-1} .

2.6 Electroconductivity measurement of $[C_n\text{Empy}][\text{Br}]$

The electrical conductivity of the $[C_n\text{Empy}][\text{Br}]$ were evaluated by a high precision conductometer (DDS-307, China). All samples were conducted to control the temperature by a water bath (temperature control accuracy: ± 0.01 K, Guning SC-30, China). All samples were measured were repeated at least 3 times until the measuring results deviation was within ± 0.01 $\mu\text{S cm}^{-1}$.

3. Results and discussion

3.1 Thermal stability analysis

The thermal stability of the $[C_n\text{Empy}][\text{Br}]$ have been measured by TG and DSC (Fig. S4 and S5†). TG analysis shows that all ester-functionalized ILs lose weight less than 1.5% (<170 °C), which is attributed to the moisture contained in ILs and the volatilization of trace impurities. Weight loss increased gradually in the temperature range 170–225 °C, thereafter it increased rapidly with temperature. The complete decomposition of $[C_n\text{Empy}][\text{Br}]$ ($n = 10, 12, 14$) occurs above at 260 °C, indicating that the ester-functionalized ILs have high thermal stabilities (Fig. S4†). DSC analysis shows that there are three stages in the phase transition of ILs (*i.e.* a crystalline (CR) phase, a liquid-crystalline (LC) phase, and an isotropic liquid (I) phase), which are marked out in Fig. S5.† Table 1 lists the analysis data from TG and DSC. As can be seen from Fig. S5,† the $[C_n\text{Empy}][\text{Br}]$ ($n = 12, 14$) have three phase transitions. It is noticed that $[C_{10}\text{Empy}][\text{Br}]$ is a continuous process from crystalline phase to isotropic liquid phase.

Table 1 Decomposition and phase transition temperatures of the ester-functionalized ILs^a

	$[C_{10}\text{Empy}][\text{Br}]$	$[C_{12}\text{Empy}][\text{Br}]$	$[C_{14}\text{Empy}][\text{Br}]$
$T_1/^\circ\text{C}$	—	50 ± 0.30	52 ± 0.26
$T_2/^\circ\text{C}$	92 ± 0.32	103 ± 0.30	100 ± 0.26
$T_3/^\circ\text{C}$	261 ± 0.32	267 ± 0.30	269 ± 0.26
$T_{\text{start}}/^\circ\text{C}$	170 ± 0.21	182 ± 0.28	168 ± 0.14
$T_{\text{onset}}/^\circ\text{C}$	220 ± 0.21	226 ± 0.28	224 ± 0.14

^a Units: T_{start} , start decomposition temperature; T_{onset} , onset decomposition temperatures; T_1 , melting points; T_2 , thermal transition temperatures; T_3 , complete decomposition temperatures.

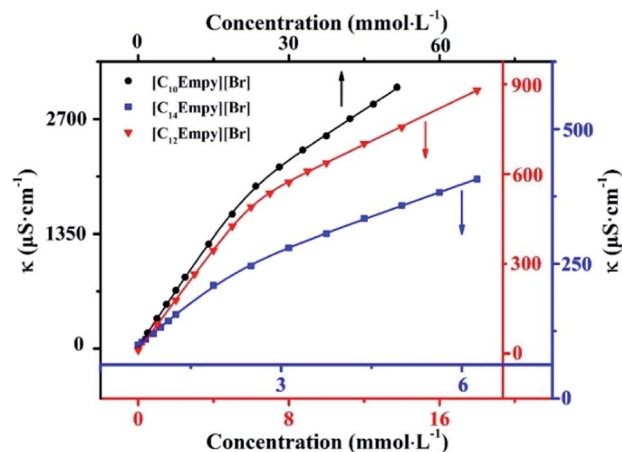


Fig. 1 Curves of the conductivity against concentration for $[C_n\text{Empy}][\text{Br}]$ ($n = 10, 12, 14$) at 298.15 K.

3.2 Conductivity measurements

Conductivity measurements is a classical method to study aggregation behavior. There are two distinct linear regions in the plot of conductivity *vs.* surfactants concentration, the breakpoint is the CMC of surfactants and the slope ratio of two linear regions is the degree of dissociation of micelles (β), respectively. Here, we use Carpena's approach to obtain the CMC value and β , which is based on non-linear fitting method to process conductivity data.^{28,29} The experimental data of electroconductivity measurement are fitted by the following equation:

$$F(x) = F(0) + S_1x + \Delta x(S_2 - S_1)\ln\left(\frac{1 + e^{(x-x_0)/\Delta x}}{1 + e^{-x_0/\Delta x}}\right) \quad (1)$$

where F_0 is the conductivity of deionized water without a surfactant, S_1 and S_2 represents slopes for under and above CMC value, respectively. X_0 is the transition state center of the curve, which is defined as the CMC value. ΔX is the width of the transition state of the curve. The ratio value of S_2/S_1 is β . The curves of conductivity against the concentration of ILSs (Fig. 1).

As shown in Fig. 1, the soaring raise of conductivity below the CMC value is attributed to the increase of free current carriers. The linear regions has a smaller slope above the CMC,

Table 2 Surfactivity parameters of *N*-alkyloxycarbonyl-3-picoline bromides^a

Surfactants	γ_{CMC}	CMC/ C_{20}	pC_{20}	π_{CMC}	Γ_{MAX}	A_{MIN}	CMC
$[C_{10}\text{Empy}][\text{Br}]$	32.1	2.00	1.94	40.0	1.29	0.128	23.3
$[C_{12}\text{Empy}][\text{Br}]$	31.0	2.04	2.58	41.1	1.63	0.102	5.37
$[C_{14}\text{Empy}][\text{Br}]$	30.1	2.16	3.06	42.0	1.95	0.085	1.88
$C_{10}\text{EPyrBr}^{25}$	—	—	2.7	41.0	—	0.071	17
$C_{12}\text{EPyrBr}^{25}$	—	—	3.5	43.0	—	0.064	4.1
$C_{14}\text{EPyrBr}^{25}$	—	—	4.0	48.0	—	0.045	0.91

^a Units: γ_{CMC} , mN m^{-1} ; π_{CMC} , mN m^{-1} ; Γ_{MAX} , $\mu\text{mol m}^{-2}$, A_{MIN} , nm^2 ; CMC, mmol L^{-1} .

two reasons can be explained for this phenomenon, (i) due to the low mobility of micelles, their contribution to charge transport is less than that of freedom ions, (ii) the effective charge of the micellar surface is reduced due to the binding of counter-ions on the micelles surface.²² Obviously, the CMC value decreased with the ester-functionalized chain length. This trend is similar to the conventional surfactants.

The CMC values of the ILSs synthesized are 22.40, 5.930 and 2.163 mmol L^{-1} , respectively. It is interesting to note that the ILSs synthesized in this work are slightly different from the previous literature²⁵ (*i.e.* the position of alkoxy and carbonyl groups in the ester chain is different). However, the CMC values of the ILSs with the same carbon atom number are quite different (Table 2), which indicates that the structure of ester-functionalized chain has a great influence on the CMC value.

For a homologous series of conventional surfactants, there is a linear relationship between the negative logarithm of CMC value and the number of carbon atoms in the hydrophobic group, which can be expressed by the following equation:^{13,18,28}

$$\log \text{CMC} = A - B \times N_c \quad (2)$$

Here A and B are constants for a homologous series of surfactants. The constant A varies with the nature and the carbon atom number of hydrophilic chain, which means hydrophilic. The higher the A value is, the stronger the hydrophilicity is, and the weaker the micellar formation ability is. The constant B is related to the hydrophobicity of the surfactants. N_c is the carbon atoms number of the hydrophobic group. As can be seen from Fig. 2, there is a linear relationship between the length of ester functional chain and CMC value, the CMC values of other homologous series ester functional surfactants can be derived from this relation. The values of A , B and coefficient of determination (R^2) for $[C_n\text{Empy}][\text{Br}]$ ($n = 10, 12, 14$) in water obtained from Fig. 2 are 0.8643, 0.2538 and 0.9876, respectively.

It is evident to find that the carbon number (n) of ester hydrophobic chain is linear with $\log \text{CMC}$. For $[C_n\text{Empy}][\text{Br}]$ ($n = 10, 12, 14$), the influence trend of ester hydrophobic chain

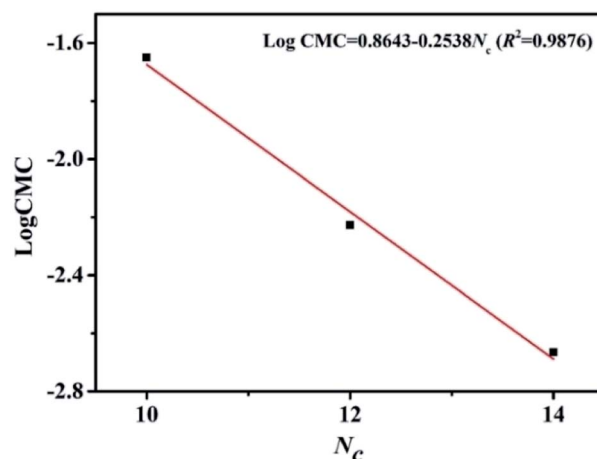


Fig. 2 The plot of $\log \text{CMC}$ vs. ester hydrophobic chain length for $[C_n\text{Empy}][\text{Br}]$.

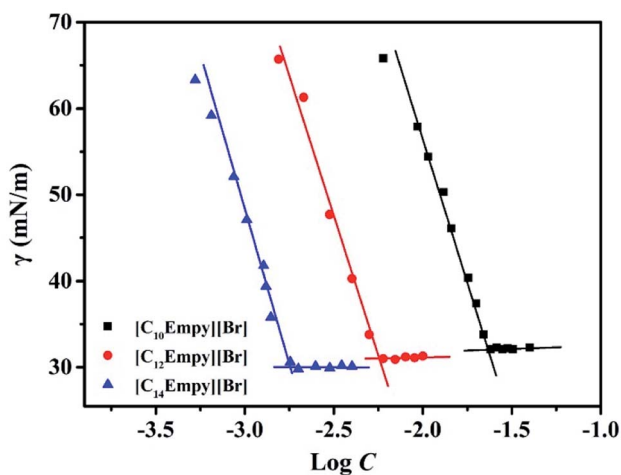


Fig. 3 The plot of surface tension against concentration of $[C_n\text{Empy}][\text{Br}]$.

length on CMC is consistent with that of conventional surfactants.^{13,18}

3.3 Surface tension measurements

In general, the surface activity of surfactants was evaluated by the measurement of surface tension. Some important surface activity parameters of surfactants can be derived. Fig. 3 shows the plot of the surface tension (γ) versus $\log[\text{surfactants concentration } (C)]$.

Fig. 3 exhibits that the γ values of ILSs solution go down dramatically with the increase of surfactants concentration, which is caused by the adsorption of ILSs molecules on the gas–water interface, and then as the surface tension stops decreasing, there is an obvious breakpoint (*i.e.* CMC), indicating that the ILSs molecule monomers aggregate into micelles.^{15,16} After the breakpoint, the γ values of ILSs solution remain almost constant with the increase of ILSs concentration. This phenomenon can be explained by the saturation of ILSs molecules at the gas–water interface.^{15,16,22} Table 2 lists some important surface activity parameters such as the surface tension at CMC (γ_{CMC}), CMC/ C_{20} ratio, adsorption efficiency (pC_{20}), surface pressure (π_{CMC}), maximum adsorption (Γ_{MAX}), and minimum surface cross-sectional area (A_{MIN}). These parameters are crucial for the study of adsorption behavior at gas–water interface. In order to clearly show that the differences in properties between the ionic liquids synthesized in this work and others previously reported, some relevant data are also listed in Table 2. It was found that the variation trend of surface activity parameters of $[C_n\text{Empy}][\text{Br}]$ is similar to that of parameter of $C_n\text{EPyrBr}$.²⁵

As can be seen from Table 2, the γ_{CMC} value of $[C_n\text{Empy}][\text{Br}]$ are 32.1, 31.0 and 30.1 mN m^{-1} , respectively. The CMC/ C_{20} ratio is generally used to evaluate the relative effects of some structural or environmental factors on micellization and on adsorption. The CMC/ C_{20} ratio can explain the reason declining trend of the γ_{CMC} value with increasing chain length. A larger CMC/ C_{20} ratio signifies a greater tendency to reduce the γ value.

Compares to other ester functionalized ILSs, $[C_{14}\text{Empy}][\text{Br}]$ has a higher ability to reduce the γ value.

The surface activity of ILSs solutions can be characterized by the adsorption efficiency (pC_{20}) and the surface pressure (π_{CMC}). The adsorption efficiency can be calculated by the following equation:^{18,27,28}

$$pC_{20} = -\log C_{20} \quad (3)$$

where C_{20} is the surfactants concentration that reducing the γ value of the water by 20 mN m^{-1} . The pC_{20} value indicates the adsorption efficiency of surfactants. The bigger pC_{20} value means that the more the surfactants adsorb at the gas–water interface and reduce the γ value more efficiently. The pC_{20} value decrease in the following order: $[C_{14}\text{Empy}][\text{Br}] > [C_{12}\text{Empy}][\text{Br}] > [C_{10}\text{Empy}][\text{Br}]$. Evidently, with the increase the length of ester-functionalized chain, the pC_{20} value shows a higher adsorption efficiency.

The surface pressure (π_{CMC}) is the surface pressure at the CMC value, which can be calculated by following equation:^{18,27,28}

$$\pi_{\text{CMC}} = \gamma_0 - \gamma_{\text{CMC}} \quad (4)$$

Here γ_0 is the surface tension of deionized water, which is 72.1 mN m^{-1} , γ_{CMC} is the surface tension at CMC value. The results show that the π_{CMC} value increase in the order of $[C_{10}\text{Empy}][\text{Br}] < [C_{12}\text{Empy}][\text{Br}] < [C_{14}\text{Empy}][\text{Br}]$. Comparing the efficiency of adsorption and the effectiveness of $[C_n\text{Empy}][\text{Br}]$ to $C_n\text{EPyrBr}$. It is clear that the position conversion of alkoxy and carbonyl groups in the ester chain has a great influence on the surface activity, $C_n\text{EPyrBr}$ possess a higher ability to reduce the surface tension of pure water than $[C_n\text{Empy}][\text{Br}]$.

The maximum surface excess (Γ_{MAX}) and the minimum surface cross sectional area (A_{MIN}) of the ILSs are calculated by the following eqn (5) and (6), respectively.^{18,27,28}

$$\Gamma_{\text{MAX}} = -\frac{1}{nRT} \left(\frac{d\gamma}{d \log C} \right)_{T,P} \quad (5)$$

$$A_{\text{MIN}} = \frac{1}{N_A \Gamma_{\text{MAX}}} \quad (6)$$

Here R is the universal gas constant ($8.314 \text{ J mol}^{-1} \text{ K}^{-1}$), N_A is the Avogadro's constant (6.023×10^{23}), T is the Kelvin temperature, $(d\gamma/d \log C)$ is the slope of γ versus $\log C$, n is taken to be 2 since there is one counter ion that is associated with one ionic head group. The results show that the Γ_{MAX} value increases, A_{MIN} value decreases by the ester-functionalized group length increase, which indicates the longer ester-functionalized chain can make the $[C_n\text{Empy}][\text{Br}]$ molecules packing more closer.¹⁷

3.4 Temperature dependence of CMC

The curves of conductivity at different concentrations for $[C_n\text{Empy}][\text{Br}]$ and the correlations between CMC and temperature are shown in Fig. 4. The CMC and β value at different temperatures analyzed based on Fig. 4 are shown in Table 3. The results show that the CMC values change with temperature in

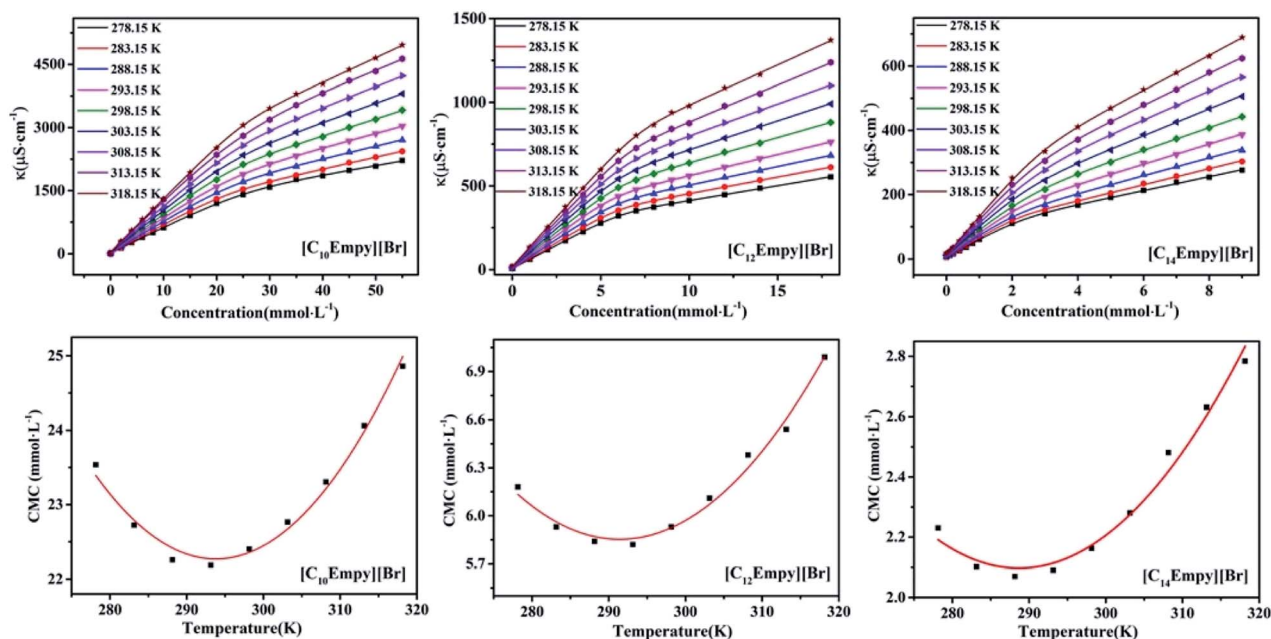


Fig. 4 The plot of conductivity vs. concentration of $[C_n\text{Empy}][\text{Br}]$ at different temperatures and the curves of CMC value vs. temperature of $[C_n\text{Empy}][\text{Br}]$ at different temperatures.

a typical U-shape (*i.e.* the CMC values initially decrease and then reach a least value (CMC*) at a certain temperature (T^*). After the T^* , the CMC values increase). The CMC *versus* temperatures

curves conform to a quadratic function, the coefficients of the curves, T^* and CMC* are listed in Table S1.† This phenomenon can be explained by two opposite effects that influence the

Table 3 The thermodynamic parameters of $[C_n\text{Empy}][\text{Br}]^a$

Surfactants	T	CMC	β	$\Delta G_{\text{mic}}^\theta$	$\Delta H_{\text{mic}}^\theta$	$\Delta S_{\text{mic}}^\theta$	$T\Delta S_{\text{mic}}^\theta$
$[C_{10}\text{Empy}][\text{Br}]$	278.15	23.54	0.360	-29.49	6.281	0.128	35.60
	283.15	22.72	0.378	-29.78	4.336	0.120	33.98
	288.15	22.26	0.398	-30.01	2.286	0.112	32.27
	293.15	22.19	0.414	-30.24	0.1396	0.104	30.49
	298.15	22.40	0.430	-30.41	-2.112	0.095	28.32
	303.15	22.76	0.445	-30.56	-4.472	0.086	26.07
	308.15	23.31	0.457	-30.73	-6.953	0.077	23.73
	313.15	24.06	0.457	-31.10	-9.646	0.068	21.29
	318.15	24.83	0.459	-31.43	-12.44	0.060	19.09
$[C_{12}\text{Empy}][\text{Br}]$	278.15	6.18	0.321	-35.34	7.116	0.149	42.56
	283.15	5.93	0.323	-36.09	4.580	0.140	40.77
	288.15	5.84	0.323	-36.79	1.858	0.131	38.61
	293.15	5.82	0.325	-37.40	-1.061	0.122	36.35
	298.15	5.93	0.335	-37.73	-4.158	0.111	33.69
	303.15	6.11	0.341	-38.10	-7.441	0.101	30.62
	308.15	6.38	0.348	-38.38	-10.91	0.090	27.43
	313.15	6.54	0.357	-38.69	-14.54	0.079	24.11
	318.15	6.99	0.357	-39.02	-18.45	0.067	20.68
$[C_{14}\text{Empy}][\text{Br}]$	278.15	2.23	0.297	-49.86	8.487	0.174	48.40
	283.15	2.09	0.304	-40.65	4.749	0.160	45.30
	288.15	2.07	0.319	-41.06	0.759	0.145	41.78
	293.15	2.09	0.324	-41.60	-3.463	0.130	38.12
	298.15	2.16	0.335	-41.90	-7.923	0.114	33.99
	303.15	2.28	0.339	-42.27	-12.67	0.098	29.71
	308.15	2.48	0.347	-42.41	-17.66	0.080	24.65
	313.15	2.63	0.348	-42.82	-23.00	0.063	19.73
	318.15	2.78	0.350	-43.21	-28.64	0.046	14.63

^a Units: T , K; CMC, mmol L^{-1} ; $\Delta G_{\text{mic}}^\theta$, kJ mol^{-1} ; $\Delta H_{\text{mic}}^\theta$, kJ mol^{-1} ; $\Delta S_{\text{mic}}^\theta$, $\text{kJ mol}^{-1} \text{K}^{-1}$; $T\Delta S_{\text{mic}}^\theta$, kJ mol^{-1} .

micellar formation.³⁰ The first effect is related to the hydration of polar groups of surfactant molecules, which plays a key role in the low temperature range, where hydrogen bonds are easier to form and the strong hydration of polar heads is not conducive to the formation of micelles. The increase in temperature leads to a decrease in the hydration of polar groups, enabling micelles to form at lower concentrations. The second effect is related to hydrophobic hydration of alkyl chains, which alters the structure of the water around the hydrophobic tail. It is well known that the structure of water is strongly dependent on temperature. Therefore, with the increase of temperature, the water structure around the hydrophobic chain becomes loose, and the effect of hydrophobic interaction becomes weaker. This phenomenon shifts the micellar process to a higher concentration range. Competition between these two effects is responsible for the observed U-shaped. Generally for a homologous series of ionic surfactants, T^* decrease with the increase of the hydrophobicity chain of surfactants, and the range of T^* is 273–313 K.^{31–33} The variation of T^* with ester chain length was similar to that of ionic surfactants, which ranges in 288–294 K.

3.5 Thermodynamic of micellization

The thermodynamic parameters of micellization can be calculated by the CMC values and β in different temperatures. According to the charged pseudo-phase separation model,^{34–36} the standard Gibbs free energy can be obtained by following equation:^{15,17}

$$\Delta G_{\text{mic}}^{\theta} = RT \times (2 - \beta) \times \ln X_{\text{cmc}} \quad (7)$$

where X_{cmc} is CMC in mole fraction, $X_{\text{cmc}} = \text{CMC}/55.4$, where CMC is in mol L⁻¹, 55.4 means that 1 L of water corresponding to 55.4 mol of water. The standard enthalpy ($\Delta H_{\text{mic}}^{\theta}$) and the standard entropy ($\Delta S_{\text{mic}}^{\theta}$) can be derived by following equation:¹⁷

$$\Delta H_{\text{mic}}^{\theta} = -RT^2 \times (2 - \beta) \times \left[\frac{\partial(\log X_{\text{cmc}})}{\partial T} \right] \quad (8)$$

$$\Delta S_{\text{mic}}^{\theta} = \frac{1}{T} (\Delta H_{\text{mic}}^{\theta} - \Delta G_{\text{mic}}^{\theta}) \quad (9)$$

The $(\partial \log X_{\text{cmc}}/\partial T)_p$ was calculated by fitting a quadratic function to the plot of $\log X_{\text{cmc}}$ vs. temperature and by taking the corresponding temperature derivative.³⁷ The correlation coefficients of quadratic function are listed in Table S2 in ESI.†

To illustrate the dependence of hydrophobic effect on temperature, we refer to an important parameter, the molar heat capacity ($\Delta C_{p,\text{mic}}^{\theta}$). This parameter is derived by the slope of the curves of $\Delta H_{\text{mic}}^{\theta}$ vs. temperature, which mainly reflects the amount of non-polar solvent accessible area buried on micellization and is highly negative.³⁷ It is worth noting that $\Delta C_{p,\text{mic}}^{\theta} < 0$, the CMC values exhibit a typical U-shaped with temperature.^{38,39}

$$\Delta C_{p,\text{mic}}^{\theta} = \left(\frac{\partial \Delta H_{\text{mic}}^{\theta}}{\partial T} \right)_p \quad (10)$$

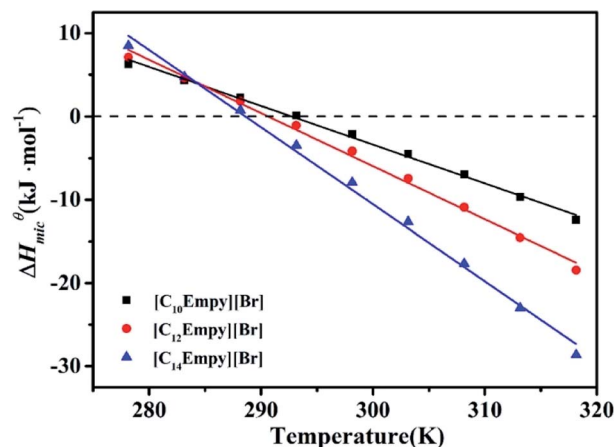


Fig. 5 The plot of temperature vs. enthalpy change for $[C_n\text{Empy}][\text{Br}]$.

Table 3 lists the $\Delta G_{\text{mic}}^{\theta}$, $\Delta H_{\text{mic}}^{\theta}$ and $\Delta S_{\text{mic}}^{\theta}$ values of ILSs at different temperatures. It is not difficult to find that all the $\Delta G_{\text{mic}}^{\theta}$ are negative, which is indicating that micellar process of ILSs molecules in water is spontaneous.

From the changes enthalpy of micellization at low/high temperatures, it can be concluded that micellization process of ILSs is endothermic at low temperatures and exothermic at high temperatures. In several ionic surfactants, the sign of $\Delta H_{\text{mic}}^{\theta}$ has a similar change with increasing temperature.^{40,41} This phenomenon can be explained by the subtle relationship between hydrophobic hydration in the nonpolar parts (endothermic) and the counterion binding upon micellization (exothermic). The temperature T_0 (ie the temperature at $\Delta H_{\text{mic}}^{\theta} = 0$) is close to T^* ,^{28,32} which is listed in Table S2.†

As shown in Fig. 5, $\Delta H_{\text{mic}}^{\theta}$ decreases with temperature resulting in a negative $\Delta C_{p,\text{mic}}^{\theta}$, this suggests that hydrophobic effect plays a key role. The hydrophobic effect is related to the water removal from the nonpolar surface in order to diminish the extent of less favourable hydrophobic hydration in comparison to clustered water in the bulk. In the aggregation

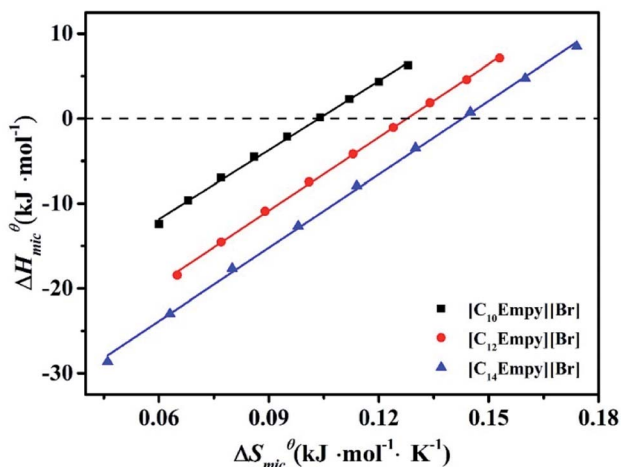


Fig. 6 Entropy–enthalpy compensation plots for $[C_n\text{Empy}][\text{Br}]$.

state, water molecules are arranged around the tail of the nonpolar surfactants at low temperature, forming an iceberg structure, or significantly reduced dynamic performance of the water molecules. Thus, the destruction of iceberg structure is a highly endothermic process.⁴² Although the endothermic contribution of hydrophobic dehydration is partially offset by the presence of favorable hydrogen bonds in the bulk, ion condensation, and other factors. The overall change enthalpy of micellar process is slightly positive at low temperatures. In addition, the water structure of the hydrophobic surface is not as stable at high temperature. Therefore, the endothermic of the hydrophobic dehydration contributes a little to the micellization and eventually the micellization becomes an exothermic process.^{27,42}

As shown in Fig. 6, the enthalpy and entropy of the micellization decrease simultaneously, which is called entropy-enthalpy compensation effect. For the micellization process, the relationship between changes in $\Delta S_{\text{mic}}^\theta$ and $\Delta H_{\text{mic}}^\theta$ can be expressed by following equation:

$$\Delta H_{\text{mic}}^\theta = \Delta H_c^\theta + T_c \Delta S_{\text{mic}}^\theta \quad (11)$$

where T_c is the compensation temperature and the slope of the eqn (11), ΔH_c^θ is the intercept of eqn (11).^{43,44} T_c can be explained by a characteristic of solute–solvent interactions, that is, as a measure of ΔH_c^θ , it describes the “desolvation” part of the micellar process and is related to the dehydration of the non-polar parts of the self-assembled molecules.⁴⁴ ΔH_c^θ represents solute–solute interactions and is considered to be an indicator of the “chemical” part of the micellar process, which is involved in the formation of monomer micelles.^{31,44}

Fig. 6 shows the entropy–enthalpy plots for ILSs, whereas the estimated values of T_c and ΔH_c^θ are listed in Table S2.† Obviously, the T_c values of ILSs are 271, 287 and 288 K, respectively. For various processes involving small molecules solutions, the range of T_c values are narrow, between 250 and 350 K.⁴³ Furthermore, for hydration to be the dominant process, T_c is 280 K.^{31,43,45,46} Therefore, according to the T_c value of the studied ILSs, the process is mainly dehydration. When the entropy contribution to micellar process is zero, $\Delta S_{\text{mic}}^\theta = 0$,⁴³ ΔH_c^θ is assumed to represent the solute–solute interaction strength at surfactants aggregation. Thus, the increase of ΔH_c^θ leads to the decrease of micellar structure stability.

As can be seen from Table S2,† it is evident that ΔH_c^θ decrease in the order of $[\text{C}_{10}\text{Empy}][\text{Br}] > [\text{C}_{12}\text{Empy}][\text{Br}] > [\text{C}_{14}\text{Empy}][\text{Br}]$, indicating that the self-assembled structures of C_{14} are more denser than that of C_{10} . This phenomenon is also common in other ionic surfactants.^{44,47}

The effect of “chemical part” of the micellar process decreases as the length of the ester functionalized chain decreases. For ionic surfactant, the alkyl group length increases by one $-\text{CH}_2-$, the ΔH_c^θ value decreases by ~ 3.9 kJ mol⁻¹; for non-ionic surfactant C_{12}E_8 , the ΔH_c^θ value decreases by ~ 2.9 kJ mol⁻¹.⁴⁴

As can be seen from Table S2,† from $[\text{C}_{10}\text{Empy}][\text{Br}]$ to $[\text{C}_{12}\text{Empy}][\text{Br}]$, the value of ΔH_c^θ decreases for 3.8 kJ mol⁻¹;

from $[\text{C}_{12}\text{Empy}][\text{Br}]$ to $[\text{C}_{14}\text{Empy}][\text{Br}]$, the value of ΔH_c^θ decreases for 2.2 kJ mol⁻¹.

For $[\text{C}_{10}\text{Empy}][\text{Br}]$ and $[\text{C}_{12}\text{Empy}][\text{Br}]$, the $T\Delta S_{\text{mic}}^\theta$ value are greater than the $-\Delta H_{\text{mic}}^\theta$ value, which indicates that the entropy gain has a great influence on the association micellization process. The micellization driving force of the $[\text{C}_{10}\text{Empy}][\text{Br}]$ and $[\text{C}_{12}\text{Empy}][\text{Br}]$ is entropy-driven.^{27,48} However, the driving force of $[\text{C}_{14}\text{Empy}][\text{Br}]$ micellization changes at high temperatures. This phenomenon can be explained as the London dispersion force plays a key role.⁴⁹

4. Conclusions

A novel series of ILSs base on *N*-alkyloxycarbonyl-3-picoline bromides have been synthesized, the micellization behavior and adsorption properties of $[\text{C}_n\text{Empy}][\text{Br}]$ ($n = 10, 12, 14$) are systematic investigated by conductivity and surface tension. The results show that $[\text{C}_n\text{Empy}][\text{Br}]$ have good thermal stability and moderate surface activity. The CMC values of $[\text{C}_n\text{Empy}][\text{Br}]$ present a U-shape with temperature. The analysis of thermodynamic parameters show that the processes of micellization of $[\text{C}_n\text{Empy}][\text{Br}]$ is spontaneous and endothermic at low temperatures and exothermic at high temperatures. According to the analysis of the enthalpy-entropy compensation curve, the compensation temperature (T_c) of investigated ILSs are 271, 287 and 288 K, respectively, indicating the domination of dehydration by micellization process at investigated ILSs. In the studied temperature range, the micellization processes of $[\text{C}_{10}\text{Empy}][\text{Br}]$ and $[\text{C}_{12}\text{Empy}][\text{Br}]$ are entropy-driven, while the micellization processes of $[\text{C}_{14}\text{Empy}][\text{Br}]$ change at high temperatures.

Author contributions

Dong Fu: writing – review & editing, methodology. Xiaoru Gao: investigation, resources. Jue Wang: resources, writing – original draft. Haijian Jiang: formal analysis. Mingming Zheng: investigation, formal analysis. Peng Li: investigation, resources. Bo Huang: investigation, Resources. Kan Kan: writing – review & editing, supervision. Xiaochen Zhang: writing – review & editing, supervision.

Conflicts of interest

There are no conflicts to declare.

Acknowledgements

This work was supported by the Youth Innovation Foundation of Heilongjiang Academy of Sciences (CXMS2019GJS01, CXJQ2022GJS01), the Natural Science Foundation of Heilongjiang Province (LH2019B030) and the Key Research and Development Project of Heilongjiang Province (GZ20210047).

References

- 1 Z. M. Xue, L. Qin, J. Y. Jiang, T. C. Mu and G. H. Gao, *Phys. Chem. Chem. Phys.*, 2018, **20**, 8382–8402.

- 2 Z. Q. He and P. Alexandridis, *Phys. Chem. Chem. Phys.*, 2015, **17**, 18238–18261.
- 3 P. C. Marr and A. C. Marr, *Green Chem.*, 2016, **18**, 105–128.
- 4 N. V. Sastry, N. M. Vaghela and V. K. Aswal, *Fluid Phase Equilib.*, 2012, **327**, 22–29.
- 5 L. Q. Peng, W. Y. Yu, J. J. Xu and J. Cao, *Food Chem.*, 2018, **239**, 1075–1084.
- 6 M. Matandabuzo and P. A. Ajibade, *J. Mol. Liq.*, 2018, **268**, 284–293.
- 7 D. S. Zhao, Y. N. Wang, E. H. Duan and J. Zhang, *Fuel Process. Technol.*, 2010, **91**, 1803–1806.
- 8 M. A. Ilies, W. A. Seitz, I. Ghiviriga, B. H. Johnson, A. Miller, E. B. Thompson and A. T. Balaban, *J. Med. Chem.*, 2004, **47**, 3744–3754.
- 9 M. Boukherissa, F. Mutelet, A. Modarressi, A. Dicko, D. Dafri and M. Rogalski, *Energy Fuels*, 2009, **23**, 2557–2564.
- 10 H. Kumar and G. Kaur, *J. Mol. Liq.*, 2020, **298**, 111949–111956.
- 11 X. W. Li, Y. A. Gao, J. Liu, L. Q. Zheng, B. Chen, L. Z. Wu and C. H. Tung, *J. Colloid Interface Sci.*, 2010, **343**, 94–101.
- 12 A. Pal and A. Pillania, *J. Mol. Liq.*, 2017, **233**, 243–250.
- 13 L. J. Shi, N. Li, H. Yan, Y. A. Gao and L. Q. Zheng, *Langmuir*, 2011, **27**, 1618–1625.
- 14 M. T. Garcia, I. Ribosa, J. J. González and F. Comelles, *J. Mol. Liq.*, 2020, **303**, 112637–112649.
- 15 Y. Wei, F. Wang, Z. Q. Zhang, C. C. Ren and Y. Lin, *J. Chem. Eng. Data*, 2012, **59**, 1120–1129.
- 16 H. Ma, H. C. Ke, T. Wang, J. H. Xiao, N. Du and L. Yu, *J. Mol. Liq.*, 2017, **240**, 556–563.
- 17 M. W. Zhao and L. Q. Zheng, *Phys. Chem. Chem. Phys.*, 2011, **13**, 1332–1337.
- 18 R. A. Rahimov, G. A. Ahmadova, G. A. Ahmadova, R. K. Mammadov, N. Z. Asadova, Y. Abdullayev, M. J. Ibrahimova, A. V. Gurbanov and F. I. Zubkov, *J. Mol. Liq.*, 2021, **344**, 117783–117792.
- 19 I. Bandrés, S. Meler, B. Giner, P. Cea and C. Lafuente, *J. Solution Chem.*, 2009, **38**, 1622–1634.
- 20 H. Y. Wang, J. J. Wang, S. B. Zhang and X. P. Xuan, *J. Phys. Chem. B*, 2008, **112**, 16682–16689.
- 21 T. Singh and A. Kumar, *Colloids Surf., A*, 2008, **318**, 263–268.
- 22 P. Quagliotto, N. Barbero, C. Barolo, E. Artuso, C. Compari, E. Fiscaro and G. Viscardi, *J. Colloid Interface Sci.*, 2009, **340**, 269–275.
- 23 N. V. Sastry, N. M. Vaghela, P. M. Macwan, S. S. Soni, V. K. Aswal and A. Gibaud, *J. Colloid Interface Sci.*, 2012, **371**, 52–61.
- 24 A. Tiwari, M. Sahoo, P. Soreng and B. K. Mishra, *J. Surfactants Deterg.*, 2018, **21**, 367–373.
- 25 M. T. Garcia, I. Ribosa, L. Perez, A. Manresa and F. Comelles, *Langmuir*, 2013, **29**, 2536–2545.
- 26 P. Patial, A. Shaheen and I. Ahmad, *J. Surfactants Deterg.*, 2014, **17**, 253–260.
- 27 D. Fu, X. R. Gao, B. Huang, J. Wang, Y. Sun, W. J. Zhang, K. Kan, X. C. Zhang, Y. Xie and X. Sui, *RSC Adv.*, 2019, **9**, 28799–28807.
- 28 D. Fu, X. R. Gao, J. Wang, Y. Xie, F. Yang, X. Sui, P. Li, B. Huang, K. Kan and X. C. Zhang, *J. Dispers. Sci. Technol.*, 2021, **42**, 791–801.
- 29 P. Carpena, J. Aguiá, P. Bernaola-Galván and C. C. Ruiz, *Langmuir*, 2002, **18**, 6054–6058.
- 30 H. Piekarski and K. Łudzik, *J. Therm. Anal. Calorim.*, 2012, **110**, 263–271.
- 31 B. Šarac, Ž. Medoš, A. Cognigni, K. Bicab, L. J. Chen and M. Bešter-Rogač, *Colloids Surf., A*, 2017, **532**, 609–617.
- 32 Ž. Medoš and M. Bešter-Rogač, *J. Chem. Thermodyn.*, 2015, **83**, 117–122.
- 33 I. Čobanov, B. Šarac, Ž. Medoš, A. Tot, M. Vraneš, S. Gadžurić and M. Bešter-Rogač, *J. Mol. Liq.*, 2021, **337**, 116353–116362.
- 34 H. Kim and K. Lim, *Colloids Surf., A*, 2004, **235**, 121–128.
- 35 T. Perger and M. Bešter-Rogač, *J. Colloid Interface Sci.*, 2007, **313**, 288–295.
- 36 J. Lah, M. Bešter-Rogač, T. Perger and G. Vesnaver, *J. Phys. Chem. B*, 2006, **110**, 23279–23291.
- 37 G. H. Tao, M. Tang, L. He, S. P. Ji, F. D. Nie and M. Huang, *Eur. J. Inorg. Chem.*, 2012, **2012**, 3070–3078.
- 38 C. L. Mesa, *J. Phys. Chem.*, 1990, **94**, 323–326.
- 39 N. Muller, *Langmuir*, 1993, **9**, 96–100.
- 40 A. Kroflič, B. Šarac and M. Bešter-Rogač, *Langmuir*, 2012, **28**, 10363–10367.
- 41 A. Kroflič, B. Šarac and M. Bešter-Rogač, *J. Chem. Thermodyn.*, 2011, **43**, 1557–1563.
- 42 A. Kroflič, B. Šarac, J. Cerkovnik and M. Bešter-Rogač, *Colloids Surf., A*, 2014, **460**, 108–117.
- 43 R. Lumry and S. Rajender, *Biopolymer*, 1970, **9**, 1125–1227.
- 44 L. Chen, S. Lin and C. Huang, *J. Phys. Chem. B*, 1998, **102**, 4350–4356.
- 45 C. V. Krishnan and H. L. Friedman, *J. Solution Chem.*, 1973, **2**, 37–51.
- 46 H. L. Friedman and C. V. Krishnan, *J. Solution Chem.*, 1973, **2**, 119–140.
- 47 C. Baar, R. Buchner and W. Kunz, *J. Phys. Chem. B*, 2001, **105**, 2914–2922.
- 48 G. Z. Cao, X. F. Guo, L. H. Jia and X. H. Tian, *RSC Adv.*, 2015, **5**, 27197–27204.
- 49 S. Kumar and K. Parikh, *J. Surfactants Deterg.*, 2013, **16**, 739–749.